

## Article

# Experimental and Process Modelling Investigation of the Hydrogen Generation from Formic Acid Decomposition Using a Pd/Zn Catalyst

Sanaa Hafeez <sup>1</sup>, Iliaria Barlocco <sup>2,\*</sup>, Sultan M. Al-Salem <sup>3</sup>, Alberto Villa <sup>2</sup>, Xiaowei Chen <sup>4</sup>,  
Juan J. Delgado <sup>4</sup>, George Manos <sup>5</sup>, Nikolaos Dimitratos <sup>6</sup> and Achilleas Constantinou <sup>7,\*</sup>

- <sup>1</sup> Division of Chemical & Energy Engineering, School of Engineering, London South Bank University, London SE1 0AA, UK; hafeezs3@lsbu.ac.uk
  - <sup>2</sup> Dipartimento di Chimica, Università degli Studi di Milano, Via Golgi, 20133 Milan, Italy; alberto.villa@unimi.it
  - <sup>3</sup> Environment & Life Sciences Research Centre, Kuwait Institute for Scientific Research, P.O. Box 24885, Safat 13109, Kuwait; ssalem@kisir.edu.kw
  - <sup>4</sup> Departamento de Ciencia de los Materiales, Ingeniería Metalúrgica y Química Inorgánica, Facultad de Ciencias, Universidad de Cádiz, Campus Río San Pedro, E-11510 Puerto Real (Cádiz), Spain; xiaowei.chen@uca.es (X.C.); juanjose.delgado@uca.es (J.J.D.)
  - <sup>5</sup> Department of Chemical Engineering, University College London, London WC1E 7JE, UK; g.manos@ucl.ac.uk
  - <sup>6</sup> Dipartimento di Chimica Industriale e dei Materiali, ALMA MATER STUDIORUM Università di Bologna, Viale Risorgimento 4, 40136 Bologna, Italy; nikolaos.dimitratos@unibo.it
  - <sup>7</sup> Department of Chemical Engineering, Cyprus University of Technology, 57 Corner of Athinon and Anexartisias, Limassol 3036, Cyprus
- \* Correspondence: ilaria.barlocco@unimi.it (I.B.); a.konstantinou@cut.ac.cy (A.C.)



**Citation:** Hafeez, S.; Barlocco, I.; Al-Salem, S.M.; Villa, A.; Chen, X.; Delgado, J.J.; Manos, G.; Dimitratos, N.; Constantinou, A. Experimental and Process Modelling Investigation of the Hydrogen Generation from Formic Acid Decomposition Using a Pd/Zn Catalyst. *Appl. Sci.* **2021**, *11*, 8462. <https://doi.org/10.3390/app11188462>

Received: 20 July 2021

Accepted: 9 September 2021

Published: 12 September 2021

**Publisher's Note:** MDPI stays neutral with regard to jurisdictional claims in published maps and institutional affiliations.



**Copyright:** © 2021 by the authors. Licensee MDPI, Basel, Switzerland. This article is an open access article distributed under the terms and conditions of the Creative Commons Attribution (CC BY) license (<https://creativecommons.org/licenses/by/4.0/>).

**Abstract:** The use of hydrogen as a renewable fuel has attracted great attention in recent years. The decomposition of formic acid under mild conditions was investigated using a 2%Pd<sub>6</sub>Zn<sub>4</sub> catalyst in a batch reactor. The results showed that the conversion of formic acid increases with reaction temperature and with the formic acid concentration. A process-simulation model was developed to predict the decomposition of formic acid using 2%Pd<sub>6</sub>Zn<sub>4</sub> in a batch reactor. The model demonstrated very good validation with the experimental work. Further comparisons between the 2%Pd<sub>6</sub>Zn<sub>4</sub> catalyst and a commercial Pd/C catalyst were carried out. It was found that the 2%Pd<sub>6</sub>Zn<sub>4</sub> demonstrated significantly higher conversions when compared with the commercial catalyst.

**Keywords:** formic acid decomposition; H<sub>2</sub> production; process simulation modelling; renewable energy; green chemistry

## 1. Introduction

The use of conventional fossil fuels for energy production has led to serious global consequences for the environment and climate. Renewable fuels have gained increasing attention in recent years to combat the current climate issues. Formic acid (HCOOH) has proven immensely popular as a favourable hydrogen storage/generation material due to its high gravimetric and volumetric hydrogen capacity, ease of handling, non-toxicity, stability at room temperature, and abundant supply from the conversion of biomass and carbon dioxide (CO<sub>2</sub>) [1]. The decomposition of formic acid reaction can be conducted in a liquid phase (at temperatures lower than 373 K) as well as in a gas phase (at excess temperatures), resulting in the dehydrogenation or dehydration pathways [2]. The former produces CO<sub>2</sub> and hydrogen (H<sub>2</sub>) as products, and the latter generates carbon monoxide (CO) and water (H<sub>2</sub>O) products. Performing the reaction at high temperatures (greater than 423 K) may lead to lower selectivity in the hydrogen production, because of the reverse water–gas shift reaction. Therefore, selective catalysts for formic acid dehydrogenation under these conditions are in high demand [3].

In recent years, heterogeneous catalysts have attracted large interest for formic acid decomposition because of enhanced separability, reusability, and relatively low reaction temperatures (less than 80 °C). The heterogeneous catalysts Pd, Au, or Ag and their alloys have been commonly studied [4–21]. A variety of materials have additionally been investigated as catalyst supports for the dehydrogenation of formic acid, such as activated carbon [22–24], zeolites [16,25], amines [26–29], metal organic frameworks (MOFs) [11,13,30,31], and macroreticular resins [32–34]. The Pd/C catalyst is the most common and effective catalyst for H<sub>2</sub> production from formic acid in aqueous solution [35]. Sanchez et al. investigated the performance of a commercial 5 wt.% Pd/C catalyst for the catalytic, additive-free decomposition of formic acid at mild conditions. The catalyst displayed an excellent 99.9% H<sub>2</sub> selectivity and a high catalytic activity (TOF = 1136 h<sup>-1</sup>) at 30 °C toward the selective dehydrogenation of formic acid to H<sub>2</sub> and CO<sub>2</sub> [5].

Formic acid decomposition for H<sub>2</sub> production has recently been investigated using Pd/ZnO catalysts, which are typically used for methanol steam reforming. Bulushev et al. [3] investigated the catalytic properties of PdZn/ZnO in formic acid decomposition. In addition, these catalysts were compared with Pt/ZnO and Pd/Al<sub>2</sub>O<sub>3</sub> catalysts as well as ZnO support. The results show that the measured catalyst activity corresponds to the following sequence: Pd/Al<sub>2</sub>O<sub>3</sub> ≥ Pd/ZnO > Pt/ZnO > ZnO. The Pd/ZnO catalyst shows the highest selectivity to hydrogen (up to 99.3%). This is attributed to the PdZn alloy formation during the catalyst reduction pretreatment. Increasing the pretreatment temperature from 573 K to 773 K resulted in a significant increase in the mean size of the PdZn (PtZn) nanoparticles. However, the activity of the catalyst remains unchanged, though the hydrogen selectivity increases.

Yao et al. [35] investigated Pd-supported catalysts for enhancing the decomposition of formic acid. The porous carbon support was synthesised using zeolitic imidazole frameworks (ZIFs) as a precursor. Furthermore, the porous carbon was produced by the one-step method. By doping the Zn into the predetermined bimetallic ZnCo-ZIFs, the operation of the catalyst was enhanced. The greatest catalytic activity of the prepared catalyst (Pd/Co@CN-2), with a 2.6 nm average diameter of PdCo, was observed when the Zn/Co molar ratio was 2 and demonstrated an initial turnover frequency value (TOF) as high as 2302 h<sup>-1</sup> at 30 °C.

Ding et al. [36] investigated the synthesis of a hybrid material of Pd nanoparticles encapsulated within carbon nanotubes (CNTs) (Pd-CNTs-in). The results show that the prepared Pd-CNTs-in catalyst exhibits particularly high formic acid decomposition activity and durability at room temperature. The TOF value was found to be 1135 h<sup>-1</sup> in the first 10 min, and there was no significant decrease in the continuous three-fold recovery study. The conclusion reached is that this work can provide a promising strategy for manufacturing cost-effective and highly active Pd-based catalysts for the dehydrogenation of formic acid.

The investigation of formic acid decomposition in batch reactors is often limited by their ability to generate a continuous stream of H<sub>2</sub> for fuel cell applications. Moreover, these reactors do not permit a detailed study of the catalyst lifetime to give an indication of its long-term performance. Therefore, the study of formic acid decomposition in continuous-flow reactors is essential to the comprehensive understanding of this reaction. The decomposition of formic acid has been explored using homogeneous and heterogeneous catalysts in continuous stirred tank reactors (CSTR) [37–39].

Caiti et al. [40] investigated the production of hydrogen via the low-temperature (less than 110 °C), additive-free decomposition of formic acid over a heterogeneous Pd/C catalyst. The results show that, during continuous-flow operation, pore contamination and poisoning caused by formate ions lead to catalyst deactivation. Although these factors cause extensive deactivation in the plug-flow mode, by operating in a continuous stirred tank reactor to reduce the steady-state formic acid concentration, encouraging results can be obtained. Therefore, under mild conditions and without stoichiometric additives, the system can operate continuously for more than 2500 cycles without loss of activity.

The decomposition of formic acid has often been investigated on an experimental basis. The utilisation of software for conducting detailed numerical studies can facilitate an understanding of parameter optimisation for the decomposition of formic acid reaction. Furthermore, theoretical studies are a valuable tool to assess the validity of the experimental findings [41,42]. Hafeez and Sanchez et al. [43] investigated the liquid-phase decomposition of formic acid using a Pd/C catalyst in a packed bed microreactor. A comprehensive heterogeneous computational fluid dynamic (CFD) model was developed to validate the experimental data. The results showed that the CFD model demonstrated very good validation with the experimental work. Furthermore, the novel model could successfully depict the deactivation of the Pd/C catalyst based on the poisoning species CO. The model developed can be used to effectively predict the decomposition of formic acid in microreactors for potential fuel cell applications.

The process-simulation modelling of formic acid decomposition has not been implemented for the current reaction system, which enhances the uniqueness of the current work. Process-simulation or flowsheet modelling can offer a solid foundation based on mass and energy balances, mass and heat transfer, reaction-system modelling, and phase equilibria to simulate the decomposition of formic acid. We utilised the capabilities of Aspen Plus to develop a simple innovative reaction system by integrating the phase-equilibrium exercises. It has been observed that both CFD and process-simulation modelling have the ability to predict different reactions with similar results [44]. The production of H<sub>2</sub> from the decomposition of formic acid has been investigated using a 2%Pd<sub>6</sub>Zn<sub>4</sub> catalyst in a batch reactor. A comprehensive process-simulation model has been developed based on the batch stirred reactor to validate the experimental findings. Further studies are performed to assess the characterisation and activity of the catalyst.

## 2. Materials and Methods

### 2.1. Materials and Chemicals

Zinc Chloride (ZnCl<sub>2</sub>, 98%), potassium tetrachloropalladate (II) (K<sub>2</sub>PdCl<sub>4</sub>, 99.99%), sodium borohydride (NaBH<sub>4</sub>, 99.99%), and formic acid were obtained from Sigma-Aldrich (Haverhill, MA, USA). The materials were utilised without the need for pretreatment. Deionised water was used as the reaction solvent for the reaction. The CNF PR24-HHT (High Heat Treated carbon nanofiber) was acquired from the Applied Science Company (Cedarville, OH, USA).

### 2.2. Catalyst Preparation

The 2%Pd<sub>6</sub>Zn<sub>4</sub>@HHT catalyst was prepared using the galvanic replacement procedure employed by Liao et al. [43], modified for the Pd–Zn system. This typical method consists of a two-step synthesis. In the first part, Zn(0) was obtained using a reducing agent (NaBH<sub>4</sub>) from ZnCl<sub>2</sub> salt. The second step involves the spontaneous displacement reduction between (PdCl<sub>4</sub>)<sup>2-</sup> and Zn. First, the support (HHT-CNFs) was added in milli-Q water under sonication conditions for 40 min. Subsequently, the mixture was degassed in a vacuum and purged in N<sub>2</sub> for 1 h. After that, 20 mg of NaBH<sub>4</sub> and 3.8 mg of Zn as ZnCl<sub>2</sub> were added. The mixture was then shaken by sonication for 5 min and placed overnight in a vacuum under vigorous stirring. In the second part, 6.2 mg of Pd as K<sub>2</sub>PdCl<sub>4</sub> was added. The mixture was then vigorously stirred in vacuum for 20 min. After that, the catalyst was filtered, washed with deionised water, and dried in the oven for 48 h.

### 2.3. Catalytic Tests

The liquid-phase formic acid dehydrogenation was performed using a two-necked round-bottom flask furnished with a magnetic stirrer and reflux condenser and placed in a water bath. Usually, 10 mL of formic acid (FA) (aqueous) was loaded into the reactor. Different concentrations of the substrate solution were utilised: 0.5 M, 0.4 M, 0.3 M, 0.2 M, and 0.1 M. After the desired temperature had been reached, the catalyst (FA:metal = 2000:1 mol/mol) was inserted and the mixture was agitated at 1400 rpm. Tests

to establish the stirring rate were previously shown by our group [4]. The catalyst was also tested at various temperatures in order to study the kinetic behaviour of the catalyst, 30 °C, 40 °C, 50 °C, and 60 °C. Stability tests were performed using the procedure previously discussed, reusing the catalyst without any further purification procedure.

High-performance liquid chromatography (HPLC) was implemented to assess the conversion of formic acid. A H<sup>+</sup> chromatographic column (Alltech OA- 10,308, 300 mm 7.8 mm) was utilised with a UV detector established at 210 nm. The liquid samples of 200 µL were obtained after certain time intervals and subsequently diluted to 5 mL with a solvent of H<sub>2</sub>SO<sub>4</sub> solution (0.005 N). This isocratic effluent flow was maintained at a flow rate of 0.5 mL/min. The volume of gases, CO and CO<sub>2</sub>, was monitored and recorded using an online micro-gas chromatograph (Agilent 3000A) every 2 h. This equipment consisted of a molecular sieve module, an OV-1 module (stationary phase of polydimethylsiloxilane), and a TCD detector. The measurement of CO and CO<sub>2</sub> was achieved from calibration curves taken from commercial standards.

#### 2.4. Catalyst Characterisation

##### XPS

The XPS measurements were recorded using a thermo Scientific K-alpha+ spectrometer. The sample analysis was achieved using a monochromatic Al X-ray source running at 72 W, with the signal recorded over an oval-shape area of 600 × 400 µ. The data were recorded at 150 eV for survey scans and 40 eV for high resolution (HR) scans with 1 eV and 0.1 eV step sizes, respectively. The analysis of the data was performed using CASAXPS (v2.3.17 PR1.1), using Scofield sensitivity factors and an energy exponent of −0.6.

##### TEM

The transmission electron microscopy (TEM) experiments were completed using a double Cs aberration-corrected FEI Titan3 Themis 60–300 microscope. The microscope was equipped with a monochromator, an X-FEG gun, and a high-efficiency XEDS ChemiSTEM. This comprised four windowless SDD detectors. HR-STEM imaging was completed at 200 kV, applying a high-angle annular dark-field (HAADF) detector with a camera length of 11.5 cm. The HAADF-STEM procedure is responsive to the atomic number of the elements, in which the intensity is roughly proportional to the square of the atomic number ( $Z^2$ ), and it provides the opportunity to differentiate the small nanoparticles carried on light supports. The XEDS mappings were achieved using a beam current of 200 pA and a dwell time per pixel of 128 µs. The elemental maps were filtered using a Gaussian blur of 0.8 (Velox software) to enhance the quality of the images. Due to the STEM-HAADF images of the catalysts, the diameters of more than 200 randomly chosen metal particles were measured and the resultant metal particle size distributions (PSD) were defined. As a result, the average particle diameter ( $d$ ) was computed corresponding to the following expression:  $d = \sum n_i d_i / \sum n_i$ , where  $n_i \geq 200$ . Equally, the total metal dispersion was evaluated according to  $D = N_s / N_t$ , where  $N_s$  is the total number of surface-metal atoms and  $N_t$  is total number of atoms in the metal particle. For the particle size calculations, the ImageJ software was used.

#### 2.5. Modelling Methodology

The decomposition of formic acid reaction was modelled using the software Aspen Plus V11. The model selected to accurately predict the behaviour of the vapour–liquid equilibrium of the reaction system was the non-random two-liquid (NRTL) model [44]. The process-modelling studies were performed in a batch reactor with a 100 mL volume and a temperature range of 30–60 °C. Characteristically, 10 mL of the required concentration of formic acid was deposited into the batch reactor. The catalyst used was 2%Pd<sub>6</sub>Zn<sub>4</sub>, the formic acid/metal molar ratio was 2000:1, and the stirring rate was 1400 rpm.

The most significant feature of the NRTL method [45] is its applicability to multi-component systems, presuming that the local compositions can be depicted by a relationship similar to that acquired for binary systems [46]:

$$\frac{x_{ji}}{x_{ki}} = \left( \frac{x_j}{x_k} \right) e^{\left[ -\frac{(\alpha_{ij}g_{ji} - \alpha_{ik}g_{ki})}{RT} \right]} \quad (1)$$

where  $x_{ji}$  and  $x_{ki}$  are the mole fractions of components  $j$  and  $k$ , respectively, in the neighbourhood of molecule  $i$ ;  $g_{ji}$  and  $g_{ki}$  are the Gibbs energies of interaction for the  $j + i$  and  $k + i$  pairs; and  $\alpha_{ij}$  and  $\alpha_{ik}$  are characteristic constants of the corresponding binary mixtures.

The activity coefficients can be expressed as follows:

$$\ln \gamma_j = \left( \frac{\sum_j \tau_{ji} G_{ji} x_j}{\sum_k G_{ki} x_k} \right) + \sum_j \left\{ \left( \frac{x_j G_{ij}}{\sum_k x_k G_{kj}} \right) \cdot \left[ \tau_{ij} - \left( \frac{\sum_l x_l \tau_{lj} G_{lj}}{\sum_k x_k G_{kj}} \right) \right] \right\} \quad (2)$$

where

$$\tau_{ij} = \frac{(g_{ij} - g_{jj})}{RT} \quad (3)$$

and

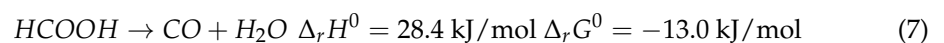
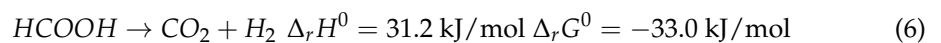
$$G_{ij} = e^{(-\alpha_{ij} \tau_{ij})} \quad (4)$$

The reactor energy balance, coupled with the material balance, can determine the heating or cooling requirements. The energy balance given for the batch stirred reactor can be expressed as follows:

$$\frac{dT}{dt} = \frac{(r_A V)(\Delta H_{RX}) - UA(T - T_a)}{\sum N_i C_{pi}} \quad (5)$$

where  $T$  is the reaction temperature,  $r_A$  is the rate of reaction,  $V$  is the volume,  $\Delta H_{RX}$  is the constant heat of reaction,  $U$  is the overall heat transfer coefficient,  $A$  is the batch reactor heat exchange area,  $T_a$  is the ambient temperature,  $N_i$  is the number of moles, and  $C_{pi}$  is the average heat capacity of species  $i$ .

The decomposition of formic acid can take place via two possible pathways dependent upon the catalyst, reaction temperature, and reactant concentrations. The dehydrogenation of formic acid is shown in Equation (1), and the dehydration reaction is shown by Equation (2). The former reaction is slightly exothermic, while the latter reaction is slightly endothermic. The type of catalyst used can determine which pathway is favoured for the decomposition of formic acid [47,48].



The rate of reaction based on the dehydrogenation of formic acid can be expressed using the Power-Law method:

$$r = k \times C^n \quad (8)$$

where  $r$  is the rate of reaction,  $k$  is the kinetic rate constant,  $C$  is the concentration of formic acid, and  $n$  is the order of reaction [5]. The estimated activation value of 22 kJ/mol was obtained for the catalyst used in this study (Pd/Zn catalyst), and the estimation was based on the experimental data of this study. The order of the reaction was accepted to be 0.2, the same as for Pd/C [5], which reproduced the experimental results satisfactorily.

### 3. Results and Discussion

The 2%Pd<sub>6</sub>Zn<sub>4</sub>@HHT catalyst was prepared using the galvanic replacement procedure employed by Liao et al. [49], modified for the Pd–Zn system. High-heat-treated carbon nanofibers (HHT-CNFs) were utilised as support for the NPs.

#### 3.1. Catalyst Characterisation

##### 3.1.1. TEM Results

The PdZn catalyst was characterised by TEM (Figure 1) to explore the bulk properties of the system (bulk zinc palladium atomic ratio, particle size distribution, and average particle size). The catalysts displayed a mean particle size of 2.1 nm, with a narrow particle size distribution (Figure 1b) and with particles well dispersed on the surface of the carbon support. On the other hand, the Pd-monometallic counterpart (1% Pd/HHT) showed a higher average particle size of 3.9 nm [4]. STEM–XEDS analysis confirmed the presence of Pd–Zn bimetallic particles with an average molar ratio of 86:14 lower than the nominal one (60:40) (Figure 1a). Figure 2 displays STEM images representing the d spacing.

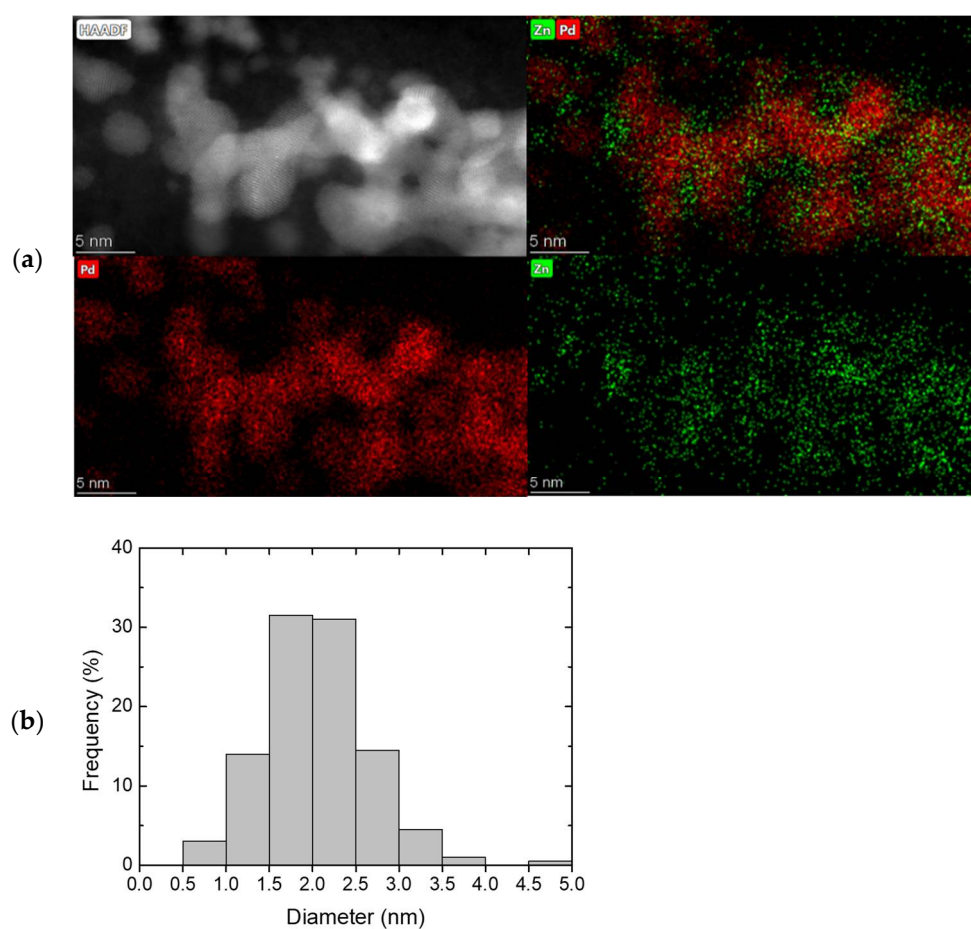


**Figure 1.** (a) STEM–XEDS of Pd<sub>6</sub>Zn<sub>4</sub> catalyst (Pd–Zn atomic ratio: 86:14) and (b) particle size distribution.

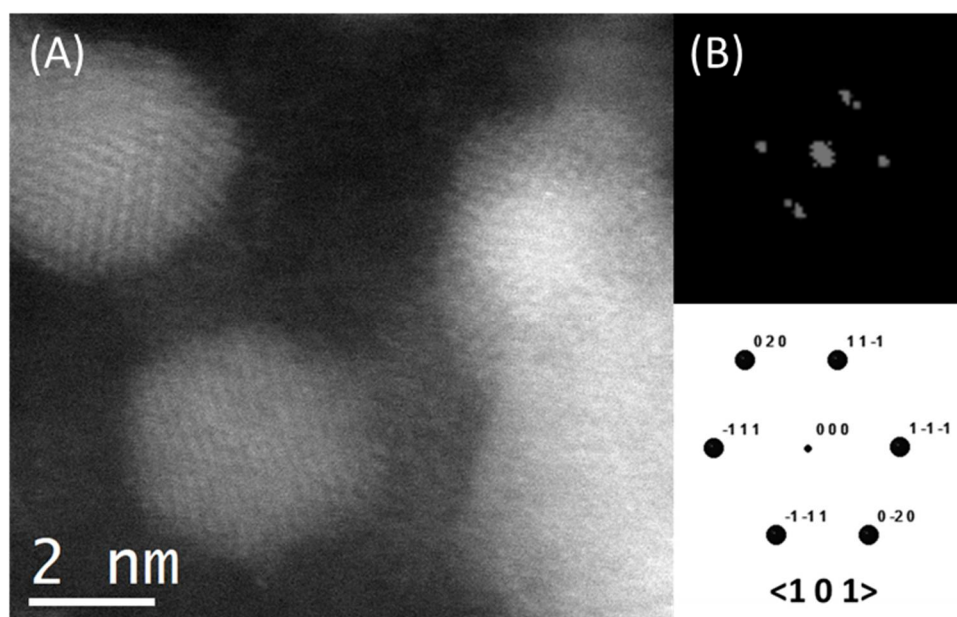


**Figure 2.** High Resolution STEM images (A), digital diffraction pattern of a selected area (B) and simulated diffraction pattern of Pd among the  $\langle 1\ 0\ 1 \rangle$  axis zone.

### 3.1.2. XPS Results

X-ray photoelectron spectroscopy (XPS) was performed on the material, obtaining information on the surface properties of the PdZn catalyst. From the XPS survey spectra, both metals were detected. The Pd/Zn atomic ratio detected by XPS is higher than the nominal one but similar to the EDX atomic ratio (Table 1), which indicates an enrichment of Pd on both surface and bulk.

**Table 1.** Results of survey spectra.

		Survey				Pd 3d		Zn 2p	Pd/Zn <sub>nom</sub>	Pd/Zn <sub>XPS</sub>	Pd/Zn <sub>EDX</sub>
		C 1s	O 1s	Pd 3d	Zn 2p	Pd(0)	Pd(II)	Zn(II)			
Pd <sub>6</sub> Zn <sub>4</sub> /HHT	B.E. (eV)	284.5	532.6	337.6	1021.6	336.0	337.6	1022.1	1.5	6.0	6.1
	% At.	95.6	3.6	0.6	0.1	9	91	100			

In the high-resolution spectra of the Pd 3d region (Figure 3), both metallic Pd and Pd oxide were detected with relative amounts of 9% and 91%, respectively. The novel catalyst shown in this study possesses a high Pd(II) content with respect to the monometallic 1% Pd/HHT, which has a Pd(0) content of 52% [4], suggesting an oxidation effect due to the presence of Zn. By analysing the high-resolution spectra of the Zn 2p region, only ZnO was detected.

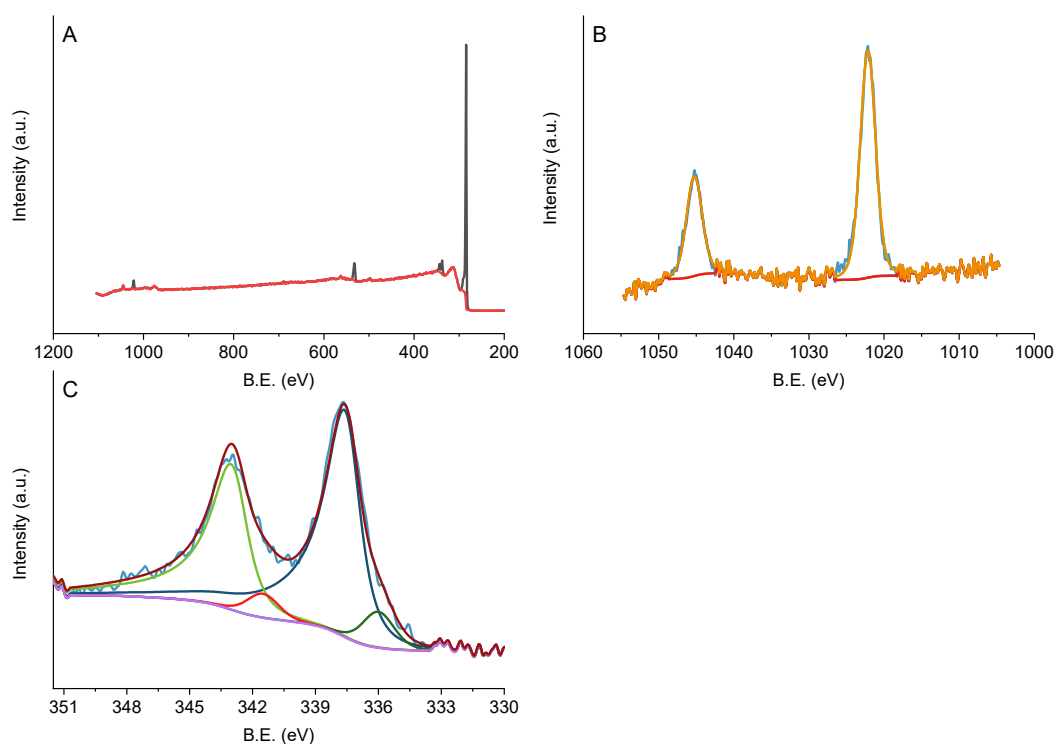


**Figure 3.** XPS (A) survey, (B) Zn 2p, and (C) Pd 3d spectra.

### 3.2. Modelling Results

#### 3.2.1. Batch Reactor Model Validation

A formic acid decomposition reaction was used as a model reaction for hydrogen production to evaluate the catalytic performance of the material. This reaction occurs in two different pathways: dehydrogenation and dehydration. The stirring rate (1400 rpm) was optimised in previous studies in order to ensure the chemical kinetic regime [4]. The experimental results for the decomposition of formic acid were compared to the process-modelling results to assess their validity. Figure 4 depicts the conversion of formic acid at varying reaction temperatures of 30–60 °C. It can be observed that the conversion increases with increasing temperatures, as expected. Furthermore, there is good validation between the experimental and theoretical results. Usually, temperatures greater than 60 °C are not investigated due to the requirement of mild operating conditions in portable devices, which utilise formic acid fuel cells. According to the Arrhenius expression,  $k = Ae^{-\frac{E_a}{RT}}$ , an apparent activation energy of approximately 22 kJ/mol was obtained for this reaction with a 2%Pd<sub>6</sub>Zn<sub>4</sub> catalyst for a batch reactor configuration. The catalytic deactivation is stronger at higher temperatures; therefore, higher reaction temperatures promote the dehydration pathway and CO formation, causing the catalyst to deactivate faster.

Kinetic profiles of the catalyst were obtained at different concentrations (0.2–0.5 M). Figure 5 demonstrates the effect of formic acid concentration on the conversion. The varying concentrations of formic acid used were 0.2–0.5 M at a reaction temperature of 30 °C and a substrate/metal molar ratio of 2000. The kinetic regime and these optimal reaction conditions were previously obtained by Sanchez et al. [5]. The results show that higher concentrations lead to higher conversions. In addition, the process-modelling studies were performed at constant reaction conditions with the experiment, and it can be concluded that there is good agreement between the experimental and theoretical data for the batch-reactor system.

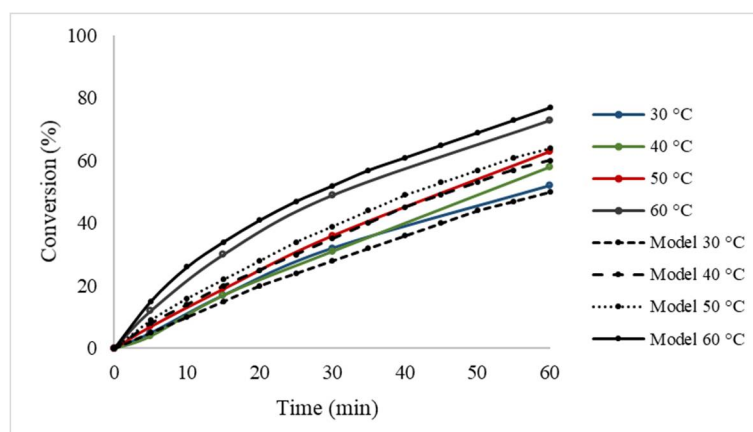


**Figure 4.** Conversion of formic acid against reaction temperature. Reaction conditions: HCOOH/metal molar ratio is 2000:1, inlet [HCOOH] = 0.5 M, rpm = 1400, catalyst 2%Pd<sub>6</sub>Zn<sub>4</sub>.

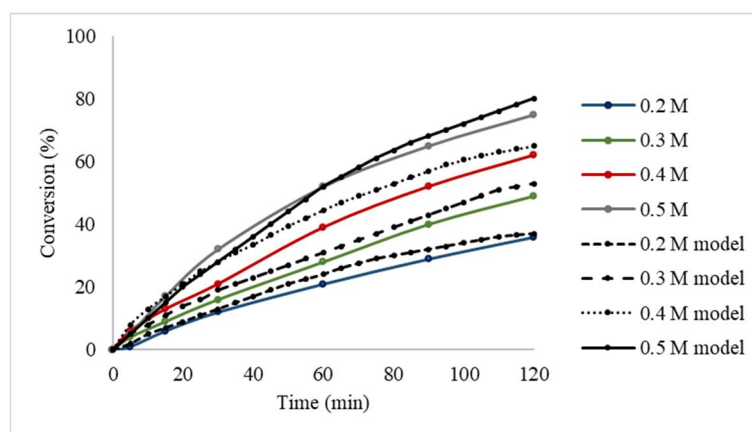


**Figure 5.** Conversion of formic acid against inlet concentration. Reaction conditions: temperature = 30 °C, HCOOH/metal molar ratio is 2000:1, rpm = 1400, catalyst 2%Pd<sub>6</sub>Zn<sub>4</sub>.

### 3.2.2. Pd/Zn vs. Pd/C Catalyst

The experimental and process-modelling results obtained using the novel 2%Pd<sub>6</sub>Zn<sub>4</sub> catalyst were compared with a commercial 5 wt.% Pd/C catalyst using a batch reactor [5]. In addition, the catalytic performance of the material presented in this work was compared with published data on 1% Pd/HHT [4,17]. The decomposition of formic acid under mild conditions using a Pd/C and 1% Pd/HHT catalyst occurred under similar conditions to those of the current work. The study was conducted using a two-necked 100 mL round-bottom flask, which was immersed in an oil bath alongside a reflux condenser and a magnetic stirrer. The reaction took place at 30 °C, and 0.5 M of aqueous formic acid solution was placed into the reactor. The substrate/metal molar ratio was 2000:1, and the stirring rate was 1400 rpm [4,5,17].

The process-simulation studies took place under constant reaction conditions for the comparison between the two catalysts to assess their performance for the reaction. From Table 2, it can be observed that, under constant reaction conditions, the performance of the novel Pd/Zn catalyst is significantly higher than that of the commercial Pd/C catalyst and of the monometallic counterpart, underlining the role of Zn in the catalytic process. As a result, the novel Pd/Zn catalyst could be utilised to enhance the decomposition of formic acid reaction. Furthermore, there is good agreement (less than 5% difference) between the process-simulation modelling and experimental data. Therefore, the theoretical models created in this study have the ability to successfully predict the decomposition of formic acid under mild conditions. A gas analysis was performed on the system using

an online micro-GC in order to calculate CO/CO<sub>2</sub> ratio, and a selectivity of 76% for the dehydrogenation reaction was obtained.

**Table 2.** Comparison between 2% Pd<sub>6</sub>Zn<sub>4</sub>, 1% Pd on nanofibers and 5 wt.% Pd on carbon. Reaction conditions: substrate/metal molar ratio: 2000:1, inlet [HCOOH] = 0.5 M, 1400 rpm 1% Pd/HHT and Pd<sub>6</sub>Zn<sub>4</sub>, 2 h reaction time.

Time (min)	X (%)				
	2% Pd <sub>6</sub> Zn <sub>4</sub> Model	2% Pd <sub>6</sub> Zn <sub>4</sub> Exp	5% Pd/C Model	5% Pd/C Exp	1% Pd Exp
0	0	0	0	0	0
5	5	5	3	5	4
15	15	17	9	10	7
30	28	32	17	16	11
60	52	52	30	30	18
90	68	65	40	40	-
120	80	75	49	46	31

#### 4. Conclusions

The decomposition of formic acid has been investigated using a novel 2%Pd<sub>6</sub>Zn<sub>4</sub> catalyst in a batch reactor. The studies were conducted experimentally, and a process-simulation model was developed to validate the results. It was found that the conversion of formic acid increases with temperatures in the range of 30–60 °C. Temperatures greater than 60 °C are not typically investigated due to the requirement of mild operating conditions for fuel cell applications. Furthermore, the formic acid conversion can be enhanced by increasing the concentration of formic acid in the batch system. For all of the parameter studies performed, the catalyst displayed no loss of activity.

The experimental and modelling data obtained for the 2%Pd<sub>6</sub>Zn<sub>4</sub> catalyst were compared with a commercial Pd/C catalyst. It was found that the novel catalyst demonstrated significantly higher conversions than the commercial catalyst under constant reaction conditions. Furthermore, the theoretical models developed to predict the decomposition of formic acid for both catalysts depicted sound validation with the experimental data, highlighting the importance of utilising computational software to further facilitate the design of experimental studies. The process-simulation-modelling methodology offered in this study can potentially offer shorter computational times and requires less computing power when compared with CFD modelling. Future research could be directed towards implementing the catalyst in a continuous flow system to allow for constant generation of hydrogen for fuel cell applications.

**Author Contributions:** Conceptualization, A.C., A.V. and N.D.; methodology, I.B., S.H., A.C., A.V. and N.D.; software, S.H., A.C. and G.M.; theoretical validation, S.H., G.M., S.M.A.-S. and A.C.; Formal analysis, I.B., A.V., N.D., X.C., J.J.D., S.H., G.M., and A.C., investigation, I.B., A.V., N.D., S.H. and A.C.; resources, I.B., A.V., S.H., X.C., J.J.D. and A.C.; writing—original draft preparation, S.H. and I.B.; writing—review and editing, S.H., I.B., A.V., N.D., X.C., J.J.D., G.M., S.M.A.-S. and A.C.; visualization, S.H., I.B., A.C., A.V., G.M., N.D.; supervision, A.C., A.V., S.M.A.-S., G.M. project administration, A.C. and A.V.; funding acquisition, A.V. and A.C. All authors have read and agreed to the published version of the manuscript.

**Funding:** This research received no external funding.

**Institutional Review Board Statement:** Not applicable.

**Informed Consent Statement:** Not applicable.

**Data Availability Statement:** Exclude this statement.

**Acknowledgments:** The authors thank London South Bank University; School of Engineering for the PhD fund that supports the work of Sanaa Hafeez.

**Conflicts of Interest:** The authors declare no conflict of interest.

## References

1. Choi, B.-S.; Song, J.; Song, M.; Goo, B.S.; Lee, Y.W.; Kim, Y.; Yang, H.; Han, S.W. Core-shell engineering of Pd-Ag bimetallic catalysts for efficient hydrogen production from formic acid decomposition. *ACS Catal.* **2018**, *9*, 819–826. [[CrossRef](#)]
2. Barlocco, I.; Capelli, S.; Lu, X.; Tumiati, S.; Dimitratos, N.; Roldan, A.; Villa, A. Role of defects in carbon materials during metal-free formic acid dehydrogenation. *Nanoscale* **2020**, *12*, 22768–22777. [[CrossRef](#)] [[PubMed](#)]
3. Bulushev, D.A.; Zacharska, M.; Beloshapkin, S.; Guo, Y.; Yuranov, I. Catalytic properties of PdZn/ZnO in formic acid decomposition for hydrogen production. *Appl. Catal. A Gen.* **2018**, *561*, 96–103. [[CrossRef](#)]
4. Sanchez, F.; Alotaibi, M.H.; Motta, D.; Chan-Thaw, C.E.; Rakotomahevitra, A.; Tabanelli, T.; Roldan, A.; Hammond, C.; He, Q.; Davies, T. Hydrogen production from formic acid decomposition in the liquid phase using Pd nanoparticles supported on CNFs with different surface properties. *Sustain. Energy Fuels* **2018**, *2*, 2705–2716. [[CrossRef](#)]
5. Sanchez, F.; Motta, D.; Roldan, A.; Hammond, C.; Villa, A.; Dimitratos, N. Hydrogen generation from additive-free formic acid decomposition under mild conditions by Pd/C: Experimental and DFT studies. *Top. Catal.* **2018**, *61*, 254–266. [[CrossRef](#)] [[PubMed](#)]
6. Sneka-Plątek, O.; Kaźmierczak, K.; Jędrzejczyk, M.; Sautet, P.; Keller, N.; Michel, C.; Ruppert, A.M. Understanding the influence of the composition of the AgPd catalysts on the selective formic acid decomposition and subsequent levulinic acid hydrogenation. *Int. J. Hydrogen Energy* **2020**, *45*, 17339–17353. [[CrossRef](#)]
7. Bao, S.; Liu, H.; Liu, Y.; Yang, W.; Wang, Y.; Yu, Y.; Sun, Y.; Li, K. Amino-functionalized graphene oxide-supported networked Pd-Ag nanowires as highly efficient catalyst for reducing Cr (VI) in industrial effluent by formic acid. *Chemosphere* **2020**, *257*, 127245. [[CrossRef](#)]
8. Qin, X.; Li, H.; Xie, S.; Li, K.; Jiang, T.; Ma, X.-Y.; Jiang, K.; Zhang, Q.; Terasaki, O.; Wu, Z. Mechanistic analysis-guided Pd-based catalysts for efficient hydrogen production from formic acid dehydrogenation. *ACS Catal.* **2020**, *10*, 3921–3932. [[CrossRef](#)]
9. Kim, Y.; Kim, S.-h.; Ham, H.C.; Kim, D.H. Mechanistic insights on aqueous formic acid dehydrogenation over Pd/C catalyst for efficient hydrogen production. *J. Catal.* **2020**, *389*, 506–516. [[CrossRef](#)]
10. Alvear, M.; Aho, A.; Simakova, I.L.; Grénman, H.; Salmi, T.; Murzin, D.Y. Aqueous phase reforming of alcohols over a bimetallic Pt-Pd catalyst in the presence of formic acid. *Chem. Eng. J.* **2020**, *398*, 125541. [[CrossRef](#)]
11. Dai, H.; Xia, B.; Wen, L.; Du, C.; Su, J.; Luo, W.; Cheng, G. Synergistic catalysis of AgPd@ ZIF-8 on dehydrogenation of formic acid. *Appl. Catal. B Environ.* **2015**, *165*, 57–62. [[CrossRef](#)]
12. Tong, F.; Lou, Z.; Liang, X.; Ma, F.; Chen, W.; Wang, Z.; Liu, Y.; Wang, P.; Cheng, H.; Dai, Y. Plasmon-induced dehydrogenation of formic acid on Pd-dotted Ag@ Au hexagonal nanoplates and single-particle study. *Appl. Catal. B Environ.* **2020**, *277*, 119226. [[CrossRef](#)]
13. Gao, S.-T.; Liu, W.; Feng, C.; Shang, N.-Z.; Wang, C. A Ag-Pd alloy supported on an amine-functionalized UiO-66 as an efficient synergetic catalyst for the dehydrogenation of formic acid at room temperature. *Catal. Sci. Technol.* **2016**, *6*, 869–874. [[CrossRef](#)]
14. Yang, L.; Hua, X.; Su, J.; Luo, W.; Chen, S.; Cheng, G. Highly efficient hydrogen generation from formic acid-sodium formate over monodisperse AgPd nanoparticles at room temperature. *Appl. Catal. B Environ.* **2015**, *168*, 423–428. [[CrossRef](#)]
15. Lv, Q.; Feng, L.; Hu, C.; Liu, C.; Xing, W. High-quality hydrogen generated from formic acid triggered by in situ prepared Pd/C catalyst for fuel cells. *Catal. Sci. Technol.* **2015**, *5*, 2581–2584. [[CrossRef](#)]
16. Navlani-García, M.; Martis, M.; Lozano-Castello, D.; Cazorla-Amorós, D.; Mori, K.; Yamashita, H. Investigation of Pd nanoparticles supported on zeolites for hydrogen production from formic acid dehydrogenation. *Catal. Sci. Technol.* **2015**, *5*, 364–371. [[CrossRef](#)]
17. Sanchez, F.; Motta, D.; Bocelli, L.; Albonetti, S.; Roldan, A.; Hammond, C.; Villa, A.; Dimitratos, N. Investigation of the catalytic performance of Pd/CNFs for hydrogen evolution from additive-free formic acid decomposition. *J. Carbon Res.* **2018**, *4*, 26. [[CrossRef](#)]
18. Barlocco, I.; Capelli, S.; Zanella, E.; Chen, X.; Delgado, J.J.; Roldan, A.; Dimitratos, N.; Villa, A. Synthesis of palladium-rhodium bimetallic nanoparticles for formic acid dehydrogenation. *J. Energy Chem.* **2021**, *52*, 301–309. [[CrossRef](#)]
19. Sanchez, F.; Bocelli, L.; Motta, D.; Villa, A.; Albonetti, S.; Dimitratos, N. Preformed Pd-Based Nanoparticles for the Liquid Phase Decomposition of Formic Acid: Effect of Stabiliser, Support and Au-Pd Ratio. *Appl. Sci.* **2020**, *10*, 1752. [[CrossRef](#)]
20. Bhalothia, D.; Huang, T.-H.; Chou, P.-H.; Chen, P.-C.; Wang, K.-W.; Chen, T.-Y. CO-Reductive and O<sub>2</sub>-Oxidative Annealing Assisted Surface Restructure and Corresponding Formic Acid Oxidation Performance of PdPt and PdRuPt Nanocatalysts. *Sci. Rep.* **2020**, *10*, 8457. [[CrossRef](#)]
21. Bhalothia, D.; Huang, T.-H.; Chou, P.-H.; Wang, K.-W.; Chen, T.-Y. Promoting formic acid oxidation performance of Pd nanoparticles via Pt and Ru atom mediated surface engineering. *RSC Adv.* **2020**, *10*, 17302–17310. [[CrossRef](#)]
22. Santos, J.L.; Megías-Sayago, C.; Ivanova, S.; Centeno, M.Á.; Odriozola, J.A. Structure-sensitivity of formic acid dehydrogenation reaction over additive-free Pd NPs supported on activated carbon. *Chem. Eng. J.* **2020**, *420*, 127641. [[CrossRef](#)]
23. Carrales-Alvarado, D.; Dongil, A.; Fernández-Morales, J.; Fernández-García, M.; Guerrero-Ruiz, A.; Rodríguez-Ramos, I. Selective hydrogen production from formic acid decomposition over Mo carbides supported on carbon materials. *Catal. Sci. Technol.* **2020**, *10*, 6790–6799. [[CrossRef](#)]

24. Wang, X.; Qi, G.-W.; Tan, C.-H.; Li, Y.-P.; Guo, J.; Pang, X.-J.; Zhang, S.-Y. Pd/C nanocatalyst with high turnover frequency for hydrogen generation from the formic acid–formate mixtures. *Int. J. Hydrogen Energy* **2014**, *39*, 837–843. [[CrossRef](#)]
25. Sun, Q.; Chen, B.W.; Wang, N.; He, Q.; Chang, A.; Yang, C.M.; Asakura, H.; Tanaka, T.; Hülsey, M.J.; Wang, C.H. Zeolite-Encaged Pd–Mn Nanocatalysts for CO<sub>2</sub> Hydrogenation and Formic Acid Dehydrogenation. *Angew. Chem.* **2020**, *132*, 20358–20366. [[CrossRef](#)]
26. Wei, R.-L.; Huang, M.; Lan, B.; Wang, C.-N.; Wang, Q.-L.; Yang, Y.-Y. Efficient decomposition of formic acid into hydrogen on Pd nanoparticles anchored in amine-pyridine polymer networks without extra additives at ambient condition. *Int. J. Hydrogen Energy* **2021**, *46*, 8469–8476. [[CrossRef](#)]
27. Biswas, S.S.; Tandrapadu, M.S.; Abinaya, E.; Eswaramoorthy, M. Deciphering the role of amine in amino silane-functionalized Pd/rGO catalyst for formic acid decomposition at room temperature. *Bull. Mater. Sci.* **2020**, *43*, 302. [[CrossRef](#)]
28. Wang, Z.; Liang, S.; Meng, X.; Mao, S.; Lian, X.; Wang, Y. Ultrasmall PdAu Alloy Nanoparticles Anchored on Amine-functionalized Hierarchically Porous Carbon as Additive-free Catalysts for Highly Efficient Dehydrogenation of Formic Acid. *Appl. Catal. B Environ.* **2021**, *291*, 120140. [[CrossRef](#)]
29. Fiorio, J.L.; Araujo, T.P.; Barbosa, E.C.; Quiroz, J.; Camargo, P.H.; Rudolph, M.; Hashmi, A.S.K.; Rossi, L.M. Gold-amine cooperative catalysis for reductions and reductive aminations using formic acid as hydrogen source. *Appl. Catal. B Environ.* **2020**, *267*, 118728. [[CrossRef](#)]
30. Ma, C.; Duan, J.; Fu, Y.; Chang, J. Hydrogen production from additive-free formic acid over highly active metal organic frameworks-supported palladium-based catalysts. *Int. J. Hydrogen Energy* **2021**, *46*, 5259–5269. [[CrossRef](#)]
31. Dai, H.; Cao, N.; Yang, L.; Su, J.; Luo, W.; Cheng, G. AgPd nanoparticles supported on MIL-101 as high performance catalysts for catalytic dehydrogenation of formic acid. *J. Mater. Chem. A* **2014**, *2*, 11060–11064. [[CrossRef](#)]
32. Mori, K.; Dojo, M.; Yamashita, H. Pd and Pd–Ag nanoparticles within a macroreticular basic resin: An efficient catalyst for hydrogen production from formic acid decomposition. *ACS Catal.* **2013**, *3*, 1114–1119. [[CrossRef](#)]
33. Mori, K.; Tanaka, H.; Dojo, M.; Yoshizawa, K.; Yamashita, H. Synergic catalysis of PdCu alloy nanoparticles within a macroreticular basic resin for hydrogen production from formic acid. *Chem. A Eur. J.* **2015**, *21*, 12085–12092. [[CrossRef](#)]
34. Mori, K.; Naka, K.; Masuda, S.; Miyawaki, K.; Yamashita, H. Palladium copper chromium ternary nanoparticles constructed in situ within a basic resin: Enhanced activity in the dehydrogenation of formic acid. *ChemCatChem* **2017**, *9*, 3456–3462. [[CrossRef](#)]
35. Yao, M.; Ye, Y.; Chen, H.; Zhang, X. Porous carbon supported Pd as catalysts for boosting formic acid dehydrogenation. *Int. J. Hydrogen Energy* **2020**, *45*, 17398–17409. [[CrossRef](#)]
36. Ding, T.-Y.; Zhao, Z.-G.; Ran, M.-F.; Yang, Y.-Y. Superior activity of Pd nanoparticles confined in carbon nanotubes for hydrogen production from formic acid decomposition at ambient temperature. *J. Colloid Interface Sci.* **2019**, *538*, 474–480. [[CrossRef](#)] [[PubMed](#)]
37. Boddien, A.; Loges, B.; Junge, H.; Gärtner, F.; Noyes, J.R.; Beller, M. Continuous hydrogen generation from formic acid: Highly active and stable ruthenium catalysts. *Adv. Synth. Catal.* **2009**, *351*, 2517–2520. [[CrossRef](#)]
38. Majewski, A.; Morris, D.J.; Kendall, K.; Wills, M. A Continuous-Flow Method for the Generation of Hydrogen from Formic Acid. *ChemSusChem* **2010**, *3*, 431–434. [[CrossRef](#)]
39. Sponholz, P.; Mellmann, D.; Junge, H.; Beller, M. Towards a practical setup for hydrogen production from formic acid. *ChemSusChem* **2013**, *6*, 1172–1176. [[CrossRef](#)]
40. Caiti, M.; Padovan, D.; Hammond, C. Continuous production of hydrogen from formic acid decomposition over heterogeneous nanoparticle catalysts: From batch to continuous flow. *ACS Catal.* **2019**, *9*, 9188–9198. [[CrossRef](#)]
41. Hafeez, S.; Aristodemou, E.; Manos, G.; Al-Salem, S.; Constantinou, A. Computational fluid dynamics (CFD) and reaction modelling study of bio-oil catalytic hydrodeoxygenation in microreactors. *React. Chem. Eng.* **2020**, *5*, 1083–1092. [[CrossRef](#)]
42. Hafeez, S.; Aristodemou, E.; Manos, G.; Al-Salem, S.; Constantinou, A. Modelling of packed bed and coated wall microreactors for methanol steam reforming for hydrogen production. *RSC Adv.* **2020**, *10*, 41680–41692. [[CrossRef](#)]
43. Hafeez, S.; Sanchez, F.; Al-Salem, S.M.; Villa, A.; Manos, G.; Dimitratos, N.; Constantinou, A. Decomposition of Additive-Free Formic Acid Using a Pd/C Catalyst in Flow: Experimental and CFD Modelling Studies. *Catalysts* **2021**, *11*, 341. [[CrossRef](#)]
44. Hafeez, S.; Mahmood, S.; Aristodemou, E.; Al-Salem, S.M.; Manos, G.; Constantinou, A. Process Simulation Modelling of the Catalytic Hydrodeoxygenation of 4-Propylguaiacol in Microreactors. *Fuels* **2021**, *3*, 16. [[CrossRef](#)]
45. Renon, H.; Prausnitz, J.M. Local compositions in thermodynamic excess functions for liquid mixtures. *AIChE J.* **1968**, *14*, 135–144. [[CrossRef](#)]
46. Juliá, J.A.; Barrero, C.R.; Corso, M.E.; del Carmen Grande, M.; Marschoff, C.M. On the application of the NRTL method to ternary (liquid + liquid) equilibria. *J. Chem. Thermodyn.* **2005**, *37*, 437–443. [[CrossRef](#)]
47. Bulushev, D.A.; Beloshapkin, S.; Ross, J.R. Hydrogen from formic acid decomposition over Pd and Au catalysts. *Catal. Today* **2010**, *154*, 7–12. [[CrossRef](#)]
48. Ting, S.-W.; Hu, C.; Pulleri, J.K.; Chan, K.-Y. Heterogeneous catalytic generation of hydrogen from formic acid under pressurized aqueous conditions. *Ind. Eng. Chem. Res.* **2012**, *51*, 4861–4867. [[CrossRef](#)]
49. Liao, M.; Hu, Q.; Zheng, J.; Li, Y.; Zhou, H.; Zhong, C.-J.; Chen, B.H. Pd decorated Fe/C nanocatalyst for formic acid electrooxidation. *Electrochim. Acta* **2013**, *111*, 504–509. [[CrossRef](#)]